# Fully Developed Hydrodynamic and Thermal Transport of Combined Pressure and Electrokinetically-driven Flow in a Microchannel With Three Immiscible Fluids

**Santanu Pramanik[1], Achintya Mukhopadhyay and Swarnendu Sen**
Department of Mechanical Engineering Jadavpur University Kolkata 700 032 India

[Received date; Accepted date] – to be inserted later

**Abstract**
**Thermally and hydrodynamically fully developed combined pressure-driven and electroosmotic flow through a channel with three immiscible fluids has been simulated for isoflux wall boundary conditions. Closed form expressions have been developed for velocity and temperature profiles and Nusselt number. The results indicate strong effects of fluid layer thickness, force fields and boundary conditions.**

## 1. INTRODUCTION

Fluid flow through microchannels is an active field of research in present days due to its increasing number of applications. MEMS sensors, micropumps, cooling of micro-electronic devices, lab-on-a-chip or bio-chip systems for drug delivery are few of the many applications that employ microfluidic transport phenomenon for their operation. Such devices generally employ motion of one or more suitable fluids through microchannels of various geometries depending entirely upon the respective application. Interestingly, flow through microchannels exhibit added features which are quite different from those in macrochannels. The development of a charged double layer at the solid liquid interface can be effectively used to transport the fluid through microchannel. Development of charged double layer can also be observed in macrochannels, but owing to their small dimension with respect to the channel width, they cannot be suitably used for transport of the fluid. On the contrary, for a microchannel, the thickness of the electrical double layer is not negligible with respect to the channel width. Hence, suitable application of electrical field may lead to the movement of these ions in the double layer and subsequently, the movement the fluid. This is particularly useful in situations where mechanical pumps cannot be used. Hence, in a microchannel, flow may be augmented both by application of pressure gradient or an electric field (electrokinetic or electroosmotic flow) or their suitable combination.

The development of electric charge at the solid liquid interface is key to electrokinetic flow. Generally when surfaces are brought into contact with an aqueous polar medium, they develop surface charge. Charging may occur due to ionization, ion adsorption and ion dissolution. The distribution of ions in the polar medium is then effected by this surface charge. Ions opposite in charge to that of the surface charge (counterions) are attracted whereas ions of similar charge (coions) are repelled. The resultant effect is the formation of an electrical double layer (EDL) in the vicinity of the charged surface where charge neutrality is absent due to greater concentration of counterions over coions. A layer of immovable counterions is present next to the charged surface known as the Stern layer. Beyond the Stern layer, the charges form a mobile diffuse layer known as the Gouy-Chapman layer. The plane

[1] Present Address: Department of Mechanical Engineering, Indian Institute of Science, Bangalore – 560 012

separating these two layers is referred to as the shear plane and the electric potential of this plane is known as the zeta potential ($\zeta$). The Stern layer and the Gouy-Chapman layer constitute the EDL. The thickness of the EDL is frequently referred to as the Debye length ($\lambda$) and is equal to the distance at which the potential of the EDL falls to ($\zeta$/e). The dimensional Debye-Huckel parameter ($\kappa$) is defined as the inverse of the Debye length.

Study of liquid flow in a microchannel due to electrokinetic effects had started as early as 1960. The early works in this field concerned fully developed flows in microchannels due to electrokinetic effects [1-3]. Yang et al. [4, 5] studied developing electroosmotic flows in microchannels. Ren and Li [6] investigated electroosmotic flows in microchannels with axially non-uniform zeta potentials and varying cross sections. Patankar and Hu [7] and Dutta et al. [8] numerically investigated electroosmotic flows in complex geometries. Yang et al [9] investigated forced convection with electrokinetic effects. Maynes and Webb [10, 11] investigated the effects of heat transfer in thermally and hydrodynamically fully developed flow in a microchannel when driven both electrokinetically and by pressure. Maynes and Webb [12] stressed the negligible effects of viscous dissipation for fully developed electrokinetic flows under typical operating conditions. Chen et al. [13] numerically investigated thermally and hydrodynamically developing flows in microchannels. Chakraborty [14] and Zade et al. [15] developed closed form solutions for hydrodynamically and thermally fully developed flow in circular microchannels with isoflux boundary conditions. Yang et al. [16] investigated the factors leading to singularities in Nusselt number for combined electrokinetiic and pressure driven flows in microchannels. Jain and Jensen [17] considered isoflux heat transfer in parallel plate microchannel neglecting the effects of Joule heating. Mukhopadhyay et al. [18] investigated the effects of asymmetries in wall boundary conditions on flow through a parallel plate microchannel when subjected to both pressure and electrokinetic effects. However these analyses are effective as long as the fluid is polar. The mechanism of electrokinetic flow is inefficient in non-polar fluids such as oils due to their low conductivity resulting in the formation of negligible amount of surface charge. The need to transport oil-like non-polar fluids results from the fact they can be efficiently used in microcooling purposes. This problem has been addressed by Brask et al. [19] and Gao et al. [20] who have proposed the use of a fluid with high electroosmotic mobility to drive the non conducting fluid. Gao et al. [21] investigated both theoretically and experimentally the way to control the interface between two fluids driven by pressure. Analysis of two-fluid system in parallel plate microchannels subject to various combinations of pressure and electric field have been reported by several researchers [22-24]. Chakraborty et al. [25] investigated the characteristics of heat transfer and Nusselt number in a two-fluid system subject to combined pressure and electrokinetic flow. Although two-fluid systems enabled the transport of non-polar fluids, the difference in fluid characteristics leads to inherent asymmetries in flow, heat transfer and resulting Nusselt number. Precise control of transport of fluids in such flow geometry may be problematic due to the asymmetry. In cooling applications differential cooling will take place at both the walls which may be undesired. Larger electric fields and pressure gradients would be required to transport the non-polar fluid due to its viscosity and contact with the wall at one end where no-slip condition exists. These conditions can be overcome if at the interface of wall and non-polar fluid, a third layer of polar fluid is inserted leading to a three fluid system and providing a symmetric geometrical layout. Transient flow characteristics of electroosmotic and pressure driven flow in three immiscible fluids confined to a rectangular microchannel have been reported by Wong et al [26]. However, detailed theoretical analysis of heat transfer and fluid in three immiscible fluid layers confined in a parallel plate microchannel subjected to pressure gradients as well as electric field is yet to be reported in literature.

The aim of the present work is to do a detailed investigation of thermally and hydrodynamically fully developed three immiscible liquids in a parallel plate microchannel with isoflux wall boundary condition. Two configurations have been studied in which the non-polar fluid is in between the polar fluids and vice versa. A comparative study of the two configurations has also been presented.

## 2. MATHEMATICAL MODEL

### 2.1 Description of the Physical Problem

Figure 1 represents a schematic of the model considered for study. The parallel plate microchannel is of total width H and consists of three fluid layers of height $H_1$, $H_2$, $H_3$ respectively. The middle fluid has been chosen to be less conducting than that of the first and third fluids. Hence the middle fluid is actually dragged by viscous action by the two end fluids. Heat flux $q''_1$ and $q''_3$ is applied to the two fluids from the lower and upper walls. Heat transfer may also take place from fluid to walls thereby providing a cooling effect. The fluid motion is augmented by the combined effects of pressure gradient and external electric field.

The major assumptions for the flow are:

a. The flow is laminar, steady, incompressible and Newtonian,
b. The flow is thermally and hydrodynamically fully developed,
c. The charge distribution follows Boltzmann distribution,
d. Local electric potential development takes place at the fluid-fluid interface,
e. Wall potentials are considered low enough for Debye-Huckel linearization to be valid,
f. The external voltage is significantly higher than the flow-induced streaming potential,
g. Thermophysical properties are constant over the ranges of temperature being encountered,
h. The channel walls are subject to constant heat flux,
i. Viscous dissipation effects are neglected.

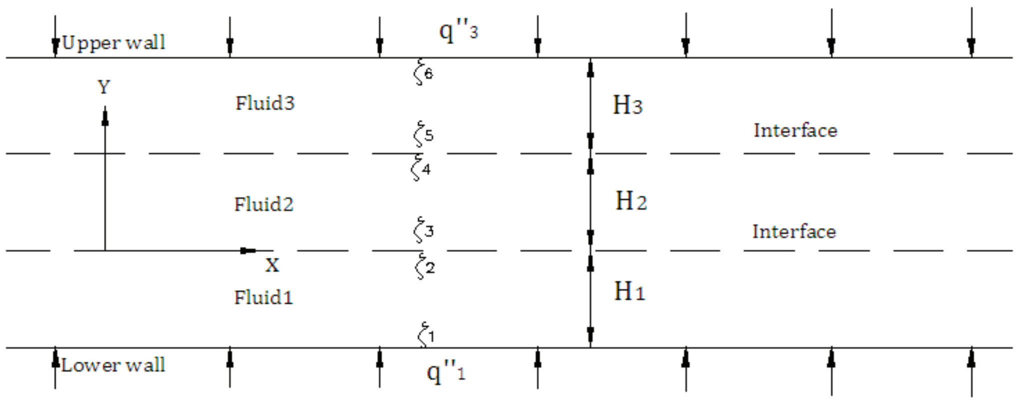


Fig. 1: Schematic of the Three Fluid Layer

### 2.2 Electrical Potential Distribution

The solid wall surface in contact with an electrolytic solution develops charge instantaneously, thereby forming the EDL. The distribution of charge in the EDL follows the Boltzmann distribution. For a solution of fully dissociated ions of two types having equal and opposite charge $z^+$ and $z^-$, the number of ions of each type are as follows;

$$n^+ = n_\infty e^{-ze\phi/k_bT};\ n^- = n_\infty e^{ze\phi/k_bT}.$$

Hence, the net charge density in the fluid is given by

$$\rho_e = (n^+ - n^-)ze = -2n_\infty ze \sinh(ze\phi/k_bT) \tag{1}$$

The electric potential distribution and the charge density are related by the Poisson-Boltzmann equation, which is of the form

$$\nabla^2\phi = -\frac{\rho_e}{\epsilon} \tag{2}$$

Since we have assumed a fully developed flow, hence $\phi = \phi(y)$ only and the potential distribution of Eq. (2) takes the following form;

$$\frac{d^2\phi}{dy^2} = -\frac{\rho_e}{\epsilon} \tag{3}$$

Combining Eqs. (1) and (3), we get the potential distribution in the fluid as

$$\frac{d^2\phi}{dy^2} = \frac{2n_\infty ze}{\epsilon}\sinh\left(ze\phi/k_bT\right) \tag{4}$$

Situations in which $|ze\phi/k_bT| < 1$, the Debye-Huckel approximation is valid. Approximating $\sinh\left(ze\phi/k_bT\right)$ as $\left(ze\phi/k_bT\right)$, Eq. (4) is modified to

$$\frac{d^2\phi}{dy^2} = \frac{2n_\infty ze}{\epsilon}\left(ze\phi/k_bT\right) = \kappa^2\phi, \text{ (say)} \tag{5}$$

where $\kappa = \sqrt{\frac{2n_\infty(ze)^2}{\epsilon k_bT}}$ is known as the Debye – Huckel parameter and is inverse of the Debye length($\lambda$). Three fluids for our present study have different physicochemical properties. Since the Debye – Huckel parameter is dependent on the fluid properties and not on the surface properties of the wall of the parallel plate; hence the potential distribution in each of the fluid will be different. The potential distributions in the three fluids can thus be given by the following differential equations;

$$\frac{d^2\phi_1}{dy^2} = \kappa_1^2\phi_1 \quad \text{for} \quad -H_1 \le y \le 0 \tag{6a}$$

$$\frac{d^2\phi_2}{dy^2} = \kappa_2^2\phi_2 \quad \text{for} \quad 0 \le y \le H_2 \tag{6b}$$

$$\frac{d^2\phi_3}{dy^2} = \kappa_3^2\phi_3 \quad \text{for} \quad H_2 \le y \le (H_2 + H_3) \tag{6c}$$

The solutions of the Eqs. (6a), (6b) and (6c) will be of the form

$$\phi_1 = C_1\cosh(\kappa_1 y) + C_2\sinh(\kappa_1 y) \tag{7a}$$

$$\phi_2 = C_1'\cosh(\kappa_2 y) + C_2'\sinh(\kappa_2 y) \tag{7b}$$

$$\phi_3 = C_1''\cosh(\kappa_3 y) + C_2''\sinh(\kappa_3 y) \tag{7c}$$

The integration constants $C_1, C_2, C_1', C_2', C_1'', C_2''$ can be evaluated by using the following boundary conditions:

$$
\begin{array}{ll}
\text{I.} & \text{at } y = H_2\,,\ \phi_2 = \zeta_4\,, \\
\text{II.} & \text{at } y = 0\,,\ \phi_2 = \zeta_3\,, \\
\text{III.} & \text{at } y = -H_1,\ \phi_1 = \zeta_1\,, \\
\text{IV.} & \text{at } y = 0\,,\ \phi_1 = \zeta_2\,, \\
\text{V.} & \text{at } y = H_2\,,\ \phi_3 = \zeta_5\,, \\
\text{VI.} & \text{at } y = H_2 + H_3\,,\ \phi_3 = \zeta_6\,,
\end{array}
\tag{8a-f}
$$

Evaluating the constants, the potential distribution in the fluid layers is obtained as;

$$\phi_1 = \frac{\zeta_2 \sinh\{\kappa_1(y+H_1)\} - \zeta_1 \sinh(\kappa_1 y)}{\sinh(\kappa_1 H_1)}\,, \quad -H_1 \le y \le 0 \tag{9a}$$

$$\phi_2 = \frac{\zeta_4 \sinh(\kappa_2 y) - \zeta_3 \sinh\{\kappa_2(y - H_2)\}}{\sinh(\kappa_2 H_2)}\,, \quad 0 \le y \le H_2 \tag{9b}$$

$$\phi_3 = \frac{\zeta_5[\sinh(\kappa_3 H_3)\cosh(\kappa_3 y) + \cosh\{\kappa_3(H_2+H_3)\}\sinh\{\kappa_3(H_2 - y)\}] - \zeta_6 \cosh(\kappa_3 H_2)\sinh\{\kappa_3(H_2 - y)\}}{\sinh(\kappa_3 H_3)\cosh(\kappa_3 H_2)}\,, H_2 \le y \le (H_2 + H_3) \tag{9c}$$

## 2.3 Velocity Distribution

The Navier-Stokes equation is used to describe the velocity characteristic of the three fluid layers in the microchannel.

$$\rho(\vec{u}\cdot\vec{\nabla})\vec{u} = -\vec{\nabla}p + \mu\nabla^2\vec{u} + \vec{F} \tag{10}$$

It consists of both pressure gradient terms as well as body force terms. The body force arises due to the imposed electric field on the fluid layers as well as the induced potential gradients in the fluid due to formation of the EDL and is given by $\vec{F} = \rho_e(\vec{E} - \vec{\nabla}\phi)$. Here F represents the net body force acting on unit volume of the fluid. However, the potential induced in the EDL is $\phi = \phi(y)$ and does not contribute to the velocity distribution in the axial directions. Also, the flow being fully developed does not have any velocity gradients in the axial direction. The pressure gradients act along axis of the microchannel. Taking all these into account, we get the equation,

$$-\frac{dp}{dx} + \mu\frac{d^2u}{dy^2} + \rho_e E = 0 \tag{11}$$

For our study, the equations describing the flow characteristics in the three fluid layers can be written as

$$0 = -\frac{dp}{dx} + \mu_1\frac{d^2u_1}{dy^2} - E\epsilon_1\frac{d^2\phi_1}{dy^2} \text{ for } -H_1 \le y \le 0 \tag{11a}$$

$$0 = -\frac{dp}{dx} + \mu_2\frac{d^2u_2}{dy^2} - E\epsilon_2\frac{d^2\phi_2}{dy^2} \text{ for } 0 \le y \le H_2 \tag{11b}$$

$$0 = -\frac{dp}{dx} + \mu_3\frac{d^2u_3}{dy^2} - E\epsilon_3\frac{d^2\phi_3}{dy^2} \text{ for } H_2 \le y \le (H_2 + H_3) \tag{11c}$$

Integrating Eqs. (11a), (11b) and (11c), the following velocity distributions are obtained:

$$u_1 = \frac{1}{\mu_1}\left(\frac{dp}{dx}\right)\frac{y^2}{2} + \frac{E\epsilon_1}{\mu_1}\phi_1 + C_3 y + C_4 \tag{12a}$$

$$u_2 = \frac{1}{\mu_2}\left(\frac{dp}{dx}\right)\frac{y^2}{2} + \frac{E\epsilon_2}{\mu_2}\phi_2 + C_3' y + C_4' \tag{12b}$$

$$u_3 = \frac{1}{\mu_3}\left(\frac{dp}{dx}\right)\frac{y^2}{2} + \frac{E\epsilon_3}{\mu_3}\phi_3 + C_3'' y + C_4'' \tag{12c}$$

The boundary conditions applicable to our flow configuration are:

$$\begin{array}{ll}
\text{I.} & \text{at } y = -H_1,\ u_1 = 0, \\
\text{II.} & \text{at } y = 0,\ \mu_1 \dfrac{du_1}{dy} = \mu_2 \dfrac{du_2}{dy}, \\
\text{III.} & \text{at } y = 0,\ u_1 = u_2, \\
\text{IV.} & \text{at } y = H_2,\ u_2 = u_3, \\
\text{V.} & \text{at } y = H_2,\ \mu_2 \dfrac{du_2}{dy} = \mu_3 \dfrac{du_3}{dy}, \\
\text{VI.} & \text{at } y = (H_2 + H_3),\ u_3 = 0,
\end{array} \tag{13}$$

The integration constants evaluated from the boundary conditions are:

$$C_3 = \frac{E\frac{\epsilon_1}{\mu_1}(\zeta_1 - \zeta_2) + E\frac{\epsilon_2}{\mu_2}(\zeta_3 - \zeta_4) + E\frac{\epsilon_3}{\mu_3}(\zeta_5 - \zeta_6) + \left(\frac{dp}{dx}\right)\left[\frac{H_1^2}{2\mu_1} - \frac{(2H_2 + H_3)H_3}{2\mu_3} - \frac{H_2^2}{2\mu_2}\right] - E\frac{H_3}{\mu_3}\left[\epsilon_1 P - \epsilon_2(Q-R) - \epsilon_3 S\right] - E\frac{H_2}{\mu_2}(\epsilon_1 P - \epsilon_2 Q)}{\left\{H_1 + \mu_1\left(\frac{H_2}{\mu_2} + \frac{H_3}{\mu_3}\right)\right\}}$$

$$\begin{aligned}
C_4 &= C_3 H_1 - E\frac{\epsilon_1}{\mu_1}\zeta_1 - \frac{1}{\mu_1}\left(\frac{dp}{dx}\right)\frac{H_1^2}{2} \\
C_3' &= C_3\frac{\mu_1}{\mu_2} + \frac{E}{\mu_2}(\epsilon_1 P - \epsilon_2 Q) \\
C_4' &= C_4 + E\left(\frac{\epsilon_1}{\mu_1}\zeta_2 - \frac{\epsilon_2}{\mu_2}\zeta_3\right) \\
C_3'' &= \frac{E}{\mu_3}(\epsilon_2 R - \epsilon_3 S) + C_3'\frac{\mu_2}{\mu_3} \\
C_4'' &= -\left[C_3''(H_2 + H_3) + E\frac{\epsilon_3}{\mu_3}\zeta_6 + \frac{1}{\mu_3}\left(\frac{dp}{dx}\right)\frac{(H_2 + H_3)^2}{2}\right], \text{ where}
\end{aligned} \tag{13a-j}$$

$$P = \frac{d\phi_1}{dy} \text{ at } y = 0,\ Q = \frac{d\phi_2}{dy} \text{ at } y = 0,\ R = \frac{d\phi_2}{dy} \text{ at } y = H_2,\ S = \frac{d\phi_3}{dy} \text{ at } y = H_2$$

## 2.4 Volume Flow Rates

The volume flow rates per unit width can be evaluated by integrating the velocity profiles in the three fluid layers, as

$$q_1 = \int_{-H_1}^{0} u_1\, dy = \frac{\left(\frac{dp}{dx}\right)H_1^3\kappa_1 \sinh(\kappa_1 H_1) + 6E\epsilon_1(\zeta_1 + \zeta_2)\{\cosh(\kappa_1 H_1) - 1\} - 3c_3 H_1^2\kappa_1\mu_1 \sinh(\kappa_1 H_1) + 6c_4 H_1\kappa_1\mu_1 \sinh(\kappa_1 H_1)}{6\kappa_1\mu_1 \sinh(\kappa_1 H_1)} \tag{14a}$$

$$q_2 = \int_0^{H_2} u_2 dy = \frac{\left(\frac{dp}{dx}\right)H_2^3\kappa_2 \sinh(\kappa_2 H_2) + 6E\epsilon_2(\zeta_3+\zeta_4)\{\cosh(\kappa_2 H_2)-1\} + 3C_3' H_2^2\kappa_2\mu_2 \sinh(\kappa_2 H_2) + 6C_4' H_2\kappa_2\mu_2 \sinh(\kappa_2 H_2)}{6\kappa_2\mu_2 \sinh(\kappa_2 H_2)} \quad (14b)$$

$$q_3 = \int_{H_2}^{H_2+H_3} u_3 dy = \frac{\left(\frac{dp}{dx}\right)\{(H_2+H_3)^3 - H_2^3\}\kappa_3 \sinh(\kappa_3 H_3) + 6E\epsilon_3(\zeta_5+\zeta_6)\{\cosh(\kappa_3 H_3)-1\} + 3C_3''(2H_2+H_3)H_3\kappa_3\mu_3 \sinh(\kappa_3 H_3) + 6C_4'' H_3\kappa_3\mu_3 \sinh(\kappa_3 H_3)}{6\kappa_3\mu_3 \sinh(\kappa_3 H_3)} \quad (14c)$$

## 2.5 Temperature Distribution

The energy conservation equation can be employed to find out the temperature distribution in the fluid layers. It takes into account the external wall heat fluxes as well as volumetric heat generation as a result of Joule heating due to the imposed electric fluid. The equation is of the following form:

$$u_1 \frac{\partial T}{\partial x} = \alpha \frac{d^2 T}{dy^2} + \frac{q_g}{\rho C_p}$$

The respective equations for our flow configuration will be

$$\rho_1 C_{p_1}(u_1 \frac{\partial T_1}{\partial x}) = k_1 \frac{d^2 T_1}{dy^2} + \sigma_1 E^2 \text{ for } -H_1 \le y \le 0 \quad (15a)$$

$$\rho_2 C_{p_2}(u_2 \frac{\partial T_2}{\partial x}) = k_2 \frac{d^2 T_2}{dy^2} + \sigma_2 E^2 \text{ for } 0 \le y \le H_2 \quad (15b)$$

$$\rho_3 C_{p_3}(u_3 \frac{\partial T_3}{\partial x}) = k_3 \frac{d^2 T_3}{dy^2} + \sigma_3 E^2 \text{ for } H_2 \le y \le (H_2 + H_3) \quad (15c)$$

For our present study, we have assumed a fully developed state with constant wall heat flux boundary condition as well as symmetric thermal boundary conditions at the two walls. These assumptions lead to

$$\frac{\partial T_1}{\partial x} = \frac{\partial T_3}{\partial x} = \frac{dT_b}{dx} = \frac{dT_w}{dx} = \text{constant} \quad (16a)$$

Here $q_1'' = q_3'' = q''$ is assumed. The energy balance of a control volume confined within the two parallel plates gives us the bulk temperature gradient as follows;

$$(\rho_1 C_{p_1} q_1 + \rho_2 C_{p_2} q_2 + \rho_3 C_{p_3} q_3) \frac{dT_b}{dx} = 2q'' + (\sigma_1 H_1 + \sigma_2 H_2 + \sigma_3 H_3) E^2 \quad (16b)$$

Eqs. (15) may be integrated and coupled with condition (16a) lead to the following temperature profiles:

$$\theta_1 = \left(\frac{y^4}{24\mu_1}\frac{dp}{dx} + \frac{E\epsilon_1\phi_1}{\mu_1\kappa_1^2} + C_3\frac{y^3}{6} + C_4\frac{y^2}{2}\right)\left(\frac{\frac{dT_b}{dx}}{\alpha_1}\right) - \frac{\sigma_1 E^2 y^2}{2k_1} + C_5 y + C_6 \quad (17a)$$

$$\theta_2 = \left(\frac{y^4}{24\mu_2}\frac{dp}{dx} + \frac{E\epsilon_2\phi_2}{\mu_2\kappa_2^2} + C_3'\frac{y^3}{6} + C_4'\frac{y^2}{2}\right)\left(\frac{\frac{dT_b}{dx}}{\alpha_2}\right) - \frac{\sigma_2 E^2 y^2}{2k_2} + C_5' y + C_6' \tag{17b}$$

$$\theta_3 = \left(\frac{y^4}{24\mu_3}\frac{dp}{dx} + \frac{E\epsilon_3\phi_3}{\mu_3\kappa_3^2} + C_3''\frac{y^3}{6} + C_4''\frac{y^2}{2}\right)\left(\frac{\frac{dT_b}{dx}}{\alpha_3}\right) - \frac{\sigma_3 E^2 y^2}{2k_3} + C_5'' y + C_6'' \tag{17c}$$

The boundary conditions are as follows:

I. at $y = -H_1,\ \theta_1 = 0,$

II. at $y = 0,\ \theta_1 = \theta_2,$

III. at $y = 0,\ k_1\frac{d\theta_1}{dy} = k_2\frac{d\theta_2}{dy},$

IV. at $y = H_2,\ \theta_2 = \theta_3,$

V. at $y = H_2,\ k_2\frac{d\theta_2}{dy} = k_3\frac{d\theta_3}{dy},$

VI. at $y = H_2 + H_3,\ \theta_3 = 0,$ (18a-f)

Although wall temperature is not specified, conditions (a) and (f) are always satisfied.

The integration constants are

$$C_5 = \frac{1}{H_1 + k_1\left(\frac{H_2}{k_2} + \frac{H_3}{k_3}\right)}\left[X_1 - X_2 + X_3 - \left(\frac{H_2}{k_2} + \frac{H_3}{k_3}\right)(X_4 - X_5) - X_6 + X_7 - \frac{H_3}{k_3}(X_8 - X_9) - X_{10}\right]$$

$$C_6 = C_5 H_1 - X_1$$

$$C_5' = \frac{k_1}{k_2}C_5 + \frac{1}{k_2}(X_4 - X_5)$$

$$C_6' = X_2 - X_3 + C_6$$

$$C_5'' = \frac{k_2}{k_3}C_5' + \frac{1}{k_3}(X_8 - X_9)$$

$$C_6'' = -X_{10} - (H_2 + H_3)\,C_5''$$

(18a-f)

For the ease of writing the integration constants use a few shorthand notations as follows.

$$X_1 = \left(\frac{H_1^4}{24\mu_1}\frac{dp}{dx} + \frac{E\epsilon_1\zeta_1}{\mu_1\kappa_1^2} + C_3\frac{H_1^3}{6} + C_4\frac{H_1^2}{2}\right)\left(\frac{\frac{dT_b}{dx}}{\alpha_1}\right) - \frac{\sigma_1 E^2 H_1^2}{2k_1}$$

$$X_2 = \left(\frac{E\epsilon_1\zeta_2}{\mu_1\kappa_1^2}\right)\left(\frac{\frac{dT_b}{dx}}{\alpha_1}\right)$$

$$X_3 = \left(\frac{E\epsilon_2\zeta_3}{\mu_2\kappa_2^2}\right)\left(\frac{\frac{dT_b}{dx}}{\alpha_2}\right)$$

$$X_4 = \frac{E\epsilon_1 k_1}{\mu_1\kappa_1^2}\left(\frac{\zeta_2\kappa_1\cosh(\kappa_1 H_1) - \zeta_1\kappa_1}{\sinh(\kappa_1 H_1)}\right)\left(\frac{\frac{dT_b}{dx}}{\alpha_1}\right)$$

$$X_5 = \frac{E\epsilon_2 k_2}{\mu_2\kappa_2^2}\left(\frac{\zeta_4\kappa_2 - \zeta_3\kappa_2\cosh(\kappa_2 H_2)}{\sinh(\kappa_2 H_2)}\right)\left(\frac{\frac{dT_b}{dx}}{\alpha_2}\right)$$

$$X_6 = \left(\frac{H_2^4}{24\mu_2}\frac{dp}{dx} + \frac{E\epsilon_2\zeta_4}{\mu_2\kappa_2^2} + C_3'\frac{H_2^3}{6} + C_4'\frac{H_2^2}{2}\right)\left(\frac{\frac{dT_b}{dx}}{\alpha_2}\right) - \frac{\sigma_2 E^2 H_2^2}{2k_2}$$

$$X_7 = \left(\frac{H_2^4}{24\mu_3}\frac{dp}{dx} + \frac{E\epsilon_3\zeta_5}{\mu_3\kappa_3^2} + C_3''\frac{H_2^3}{6} + C_4''\frac{H_2^2}{2}\right)\left(\frac{\frac{dT_b}{dx}}{\alpha_3}\right) - \frac{\sigma_3 E^2 H_2^2}{2k_3}$$

$$X_8 = k_2\left[\frac{H_2^3}{6\mu_2}\frac{dp}{dx} + \frac{E\epsilon_2}{\mu_2\kappa_2^2}\left\{\frac{\zeta_4\kappa_2\cosh(\kappa_2 H_2) - \zeta_3\kappa_2}{\sinh(\kappa_2 H_2)}\right\} + C_3'\frac{H_2^2}{2} + C_4' H_2\right]\left(\frac{\frac{dT_b}{dx}}{\alpha_2}\right) - \sigma_2 E^2 H_2$$

$$X_9 = k_3\left[\frac{H_2^3}{6\mu_3}\frac{dp}{dx} + \frac{E\epsilon_3}{\mu_3\kappa_3^2}\left\{\frac{\zeta_5\kappa_3[\sinh(\kappa_3 H_3)\sinh(\kappa_3 H_2) - \cosh\{\kappa_3(H_2+H_3)\}] - \zeta_6\kappa_3\cosh(\kappa_3 H_2)}{\sinh(\kappa_3 H_3)\cosh(\kappa_3 H_2)}\right\} + C_3''\frac{H_2^2}{2} + C_4'' H_2\right]\left(\frac{\frac{dT_b}{dx}}{\alpha_3}\right) - \sigma_3 E^2 H_2$$

$$X_{10} = \left(\frac{(H_2+H_3)^4}{24\mu_3}\frac{dp}{dx} + \frac{E\epsilon_3\zeta_6}{\mu_3\kappa_3^2} + C_3''\frac{(H_2+H_3)^3}{6} + C_4''\frac{(H_2+H_3)^2}{2}\right)\left(\frac{\frac{dT_b}{dx}}{\alpha_3}\right) - \frac{\sigma_3 E^2 (H_2+H_3)^2}{2k_3}$$

(19a-j)

All the integration constants (18a-f) and Eq. 17a, b, c define the temperature distribution in the three fluid layers.

## 2.6 Nusselt Number

The bulk mean temperature of the fluid layers is represented as

$$\theta_b = T_b - T_w = \frac{\int_{-H_1}^{0}\rho_1 C_{p_1} u_1\theta_1 dy + \int_0^{H_2}\rho_2 C_{p_2} u_2\theta_2 dy + \int_{H_2}^{H_2+H_3}\rho_3 C_{p_3} u_3\theta_3 dy}{\int_{-H_1}^{0}\rho_1 C_{p_1} u_1 dy + \int_0^{H_2}\rho_2 C_{p_2} u_2 dy + \int_{H_2}^{H_2+H_3}\rho_3 C_{p_3} u_3 dy}$$

represents the bulk mean temperature of the fluid layers. Since the convective heat transfer depends on the difference between the wall temperature and the bulk mean temperature, at steady state, the heat flux conducted at the solid fluid interface will be equal to the heat convected to the end fluid layers. So

$$h_1\theta_b = k_1\frac{d\theta_1}{dy} \text{ at } y = -H_1 \tag{20a}$$

$$h_3\theta_b = -k_3\frac{d\theta_3}{dy} \text{ at } y = H_2 + H_3 \tag{20b}$$

Defining Nusselt number as 4*(area)/ (wetted perimeter) we get

$$Nu_1 = \frac{2h_1(H_1+H_2+H_3)}{k_1} \tag{21a}$$

$$Nu_3 = \frac{2h_3(H_1+H_2+H_3)}{k_3} \tag{21b}$$

## 3. RESULTS AND DISCUSSIONS

The velocity distributions, temperature profiles and heat transfer characteristics have been studied by suitable choice of thermophysical properties of the fluid layers involved. These values do not pertain to any particular fluid, but are representative of their properties which have been chosen for various simulations. The two end fluids have suitably been chosen as conducting whereas the middle layer has been considered non-conducting. The first and third fluids are same and have the same properties, $\frac{\mu_2}{\mu_1} = 20$, $\frac{\rho_2}{\rho_1} = 1$, $\frac{k_2}{k_1} = 0.1$, $\frac{C_{p2}}{C_{p1}} = 1$. Also, we have described two non-dimensional parameters for the study of various flow situations, $P = \frac{\frac{E\epsilon_1}{\mu_1}\left(\frac{\zeta_1+\zeta_2}{2}\right) + \frac{E\epsilon_2}{\mu_2}\left(\frac{\zeta_3+\zeta_4}{2}\right) + \frac{E\epsilon_3}{\mu_3}\left(\frac{\zeta_5+\zeta_6}{2}\right)}{\left(\frac{H_1^2}{2\mu_1}+\frac{H_2^2}{2\mu_2}+\frac{H_3^2}{2\mu_3}\right)\left(\frac{dp}{dx}\right)}$ which describes the relative measure of the amount of force due to imposed electric field to that due to the pressure gradient and $S = \left(\frac{2q''}{\sigma_1 E^2 H_1 + \sigma_2 E^2 H_2 + \sigma_3 E^2 H_3}\right)$ which gives the relative measure of the amount of external heating to that of internal generation due to Joule heating. A very high value of P implies purely electroosmotic flow, whereas P = 0 implies purely pressure driven flow. By assigning various values to these non-dimensional parameters, we get a detailed insight about the effects of pressure gradient, electric field, external heat flux and Joule heating on the heat transfer characteristics.

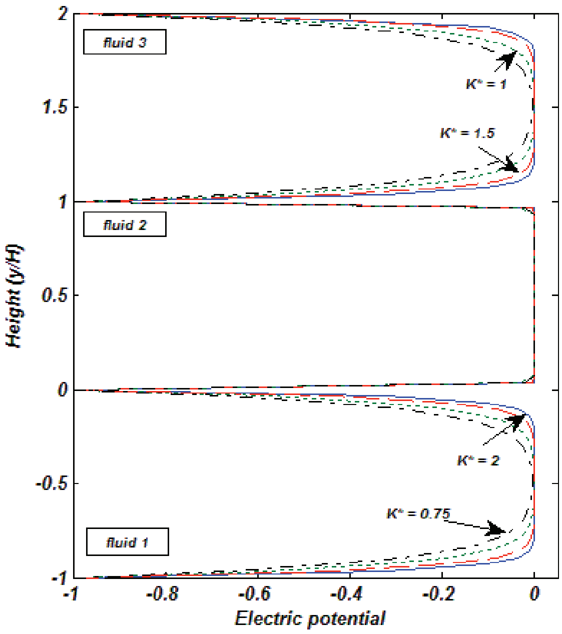


Figure 2: Electric potential distribution

### 3.1 Electric Potential Distributions

Electric potential induced in the fluid layers vary continuously with thickness of the fluid layer. This distribution is a function of the zeta potentials at the interfaces of fluids and wall and the Debye-Huckel parameter, which is the inverse of the Debye length of the fluid. We consider a $\zeta_r$ = 25 mV and the potentials are normalized with respect to this reference potential value. Also, $\zeta_1 = \zeta_2 = \zeta_3 = \zeta_4 = \zeta_5 = \zeta_6 = 25$ mV. We have also considered reference values of the Debye Huckel parameter: $\kappa_{1r} = \kappa_{3r} = 16 * 10^4\ \mathrm{m}^{-1}$ and $\kappa_{2r} = 100 * 10^4\ \mathrm{m}^{-1}$; $\kappa^* = \frac{\kappa}{\kappa_{nr}}$ where n = 1, 2, 3. With an increase in $\kappa^*$, the value of Debye length decreases which implies that the potential becomes zero nearer to the wall. For very high values of $\kappa^*$, the potential throughout the fluid almost remains zero and hence there is no substantial effect of the applied electric field on fluid flow (as in fluid 2).

For lower values of $\kappa^*$, the EDL increases in length and there may even be EDL overlap. However the treatment to such a situation is different from the one adopted here and hence the values of $\kappa^*$ have been limited so that there is no EDL overlap. Also fluid 2 has been so chosen that EDL thickness is almost zero in turn implying that the fluid is non-polar. Just the reverse configuration will be obtained when the non-polar fluid will be at the two ends and dragged by the polar fluid in the middle.

### 3.2 Velocity Distribution

For validation of the derived equations, the three fluid layers have been approximated as two fluid system assigning identical properties to second and third fluid layers and compared with the velocity distribution obtained by Chakraborty et al [25]. Other properties assigned are $\frac{\mu_2}{\mu_1} = 20, \frac{\rho_2}{\rho_1} = 1,$

$\frac{k_2}{k_1} = 0.1, \frac{C_{p2}}{C_{p1}} = 1, \frac{\epsilon_2}{\epsilon_1} = 0.5, \frac{\sigma_2}{\sigma_1} = 0.1, \zeta_1 = \zeta_2, \zeta_4 = \zeta_5 = 0, \zeta_3 = \zeta_6 = 0.5\zeta_1, H_1 = H_2 + H_3, H_2 = H_3.$

The velocity profile, shown in Fig. 3, matches not only in form but also in magnitude to the velocity profile in [25] (cf. Fig. 2 of [25]). To obtain the velocity profile for the three fluid system, the electrical properties chosen are, $\frac{\epsilon_2}{\epsilon_1} = 0, \frac{\sigma_2}{\sigma_1} = 0, \zeta_1 = \zeta_2 = \zeta_5 = \zeta_6 = \zeta_3 = \zeta_4$

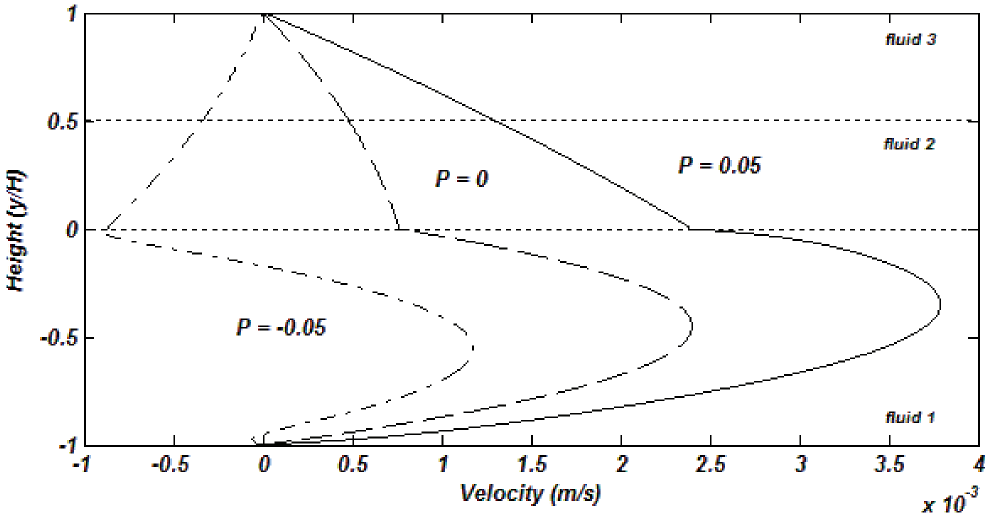


Figure 3: Validation plot for velocity profile in two fluid-layer microchannel

Figure 4 shows the velocity profiles for the three fluid layers for the non-polar fluid in the middle in Fig. 4(a) and the polar fluid in the middle in Fig. 4(b). The three curves represent three values of P. The curve with P = 0.05 is the case in which both the pressure gradient and body force due to imposed electric field act in the same direction. This results in a higher absolute velocity of the fluid layers. The middle layer being more viscous has low velocity gradient and has almost uniform velocity throughout. Hence to satisfy the shear-stress continuity, a larger velocity gradient appears in the two identical end fluid layers which are less viscous. The curve with P = 0 represents purely pressure driven flow and as such, there are no effects of electroosmotic forces. The curve with P = - 0.05 has same magnitude of pressure gradient and electric field but are oppositely directed. This results in a lower velocity and as the flow pattern indicates, there may be flow reversal for higher magnitudes of reverse electric fields or more negative values of P (as can be seen near walls in Figure 4a for P = - 0.05). Another thing that can be observed between Figure 4a and 4b is that the max velocity obtained in case of 4b is much less as compared to 4a. This can be attributed to the fact that a highly viscous fluid being near the wall in 4b, it decelerates the bulk flow because of no slip at the wall.

(4a)

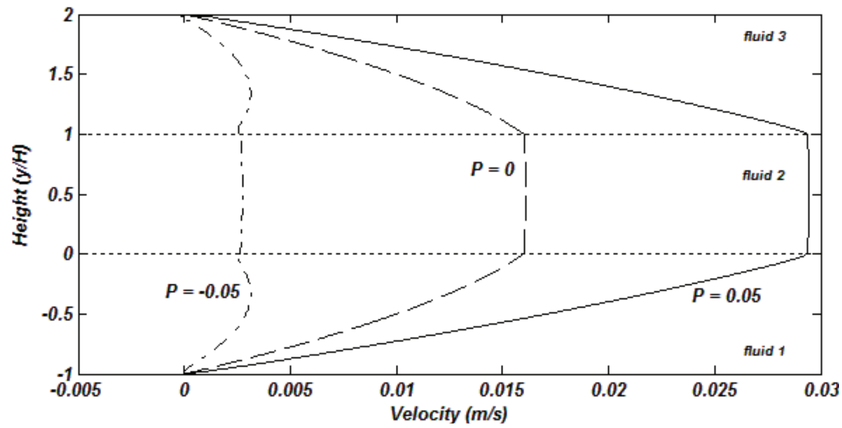


(4b)

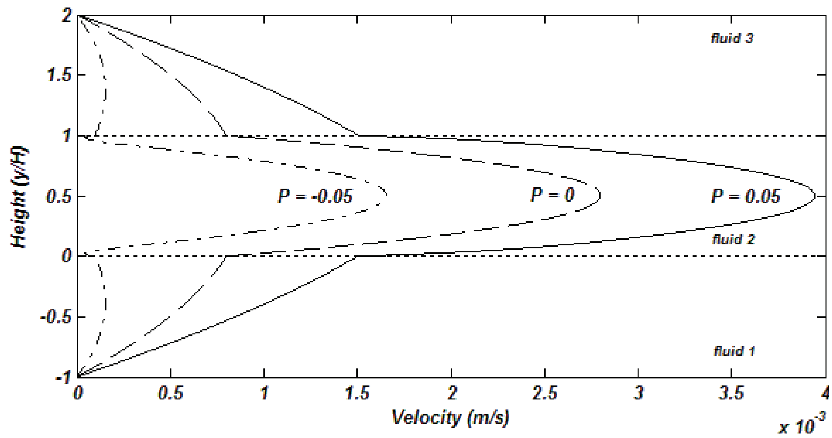


Figure 4: Velocity profile in the three fluid layers for different values of P with equal thickness of the three fluid layers (a) non-polar fluid in the middle (b) polar fluid in the middle

### 3.3 Temperature Distribution

Temperature distribution is first validated with the results of Chakraborty et al. [25] by setting identical properties to two adjacent layers of fluids. The results, shown in Fig. 5, show excellent quantative agreement with those of Ref. [25].

Having verified the temperature profiles, the temperature distribution for three fluid layers were also obtained for the above mentioned parameters and P=0.05, - 0.05.

(5a)

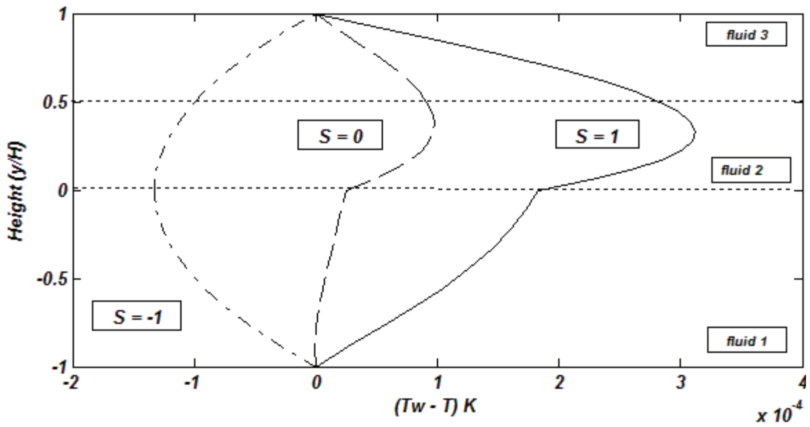


(5b)

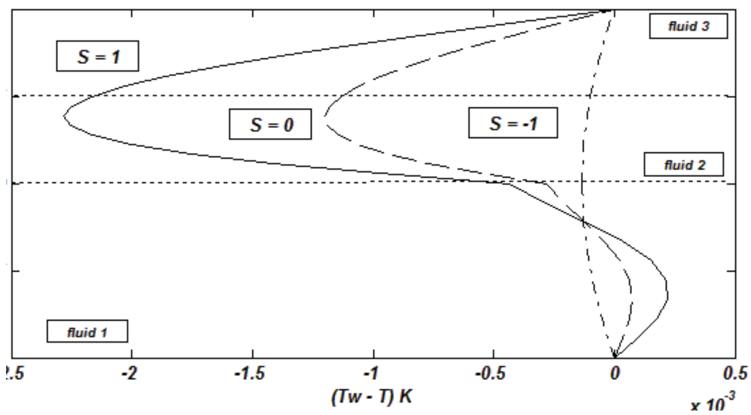


Figure 5: Validation plot for temperature profile in two fluid-layer microchannel (a) P = 0.05 (b) P = -0.05

In figure 6a, the middle fluid being non-conducting does not experience Joule heating whereas the lower end fluid layers are heated due to the electric field. This heat is conducted to the walls and gives a higher vertical temperature gradient in the end fluid layers. However, in figure 6b, reverse configurations exist. Here the middle fluid is heated by Joule heating. However as the middle fluid is of higher conductivity, it easily conducts the heat to the adjacent fluid layers. These fluid layers have low thermal conductivity and thus have a higher temperature gradient to maintain the continuity of heat fluxes.

(6a)

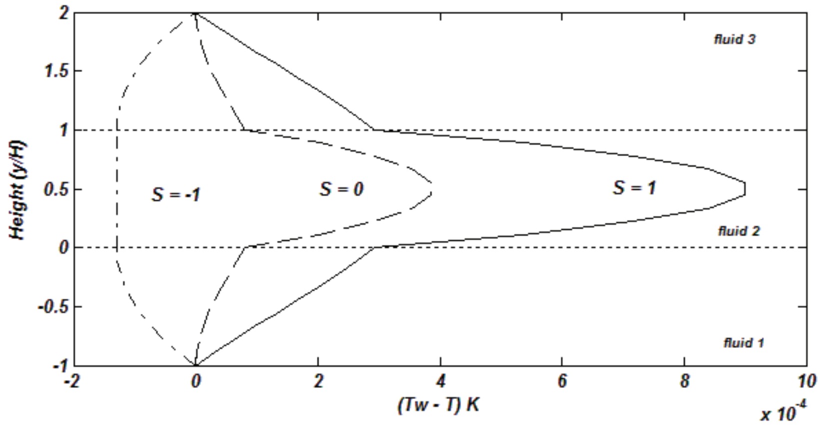


(6b)

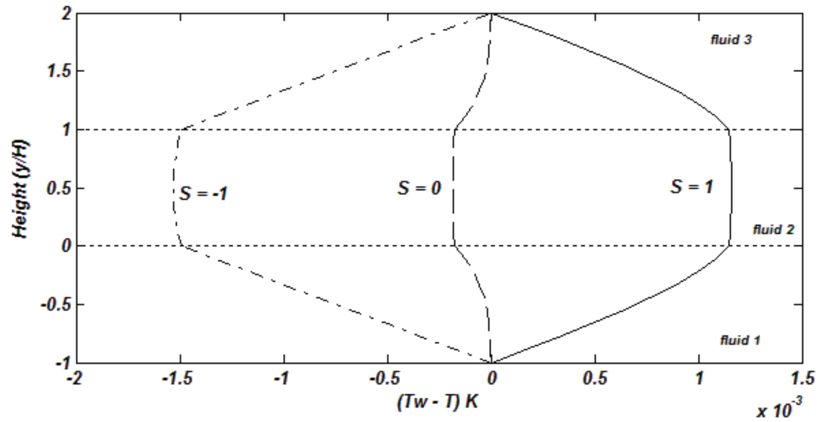


Figure 6: Plots for temperature profile with different values of S and P=0.05, (a) non polar fluid in the middle, k2/k1 = 0.1 (b) polar fluid in the middle, k1/k2 = 0.1

S = 0 represents the case of zero wall heat fluxes, as if the walls are insulated. In figure 6a, heat generated in the end fluid layers due to Joule heating is actually conducted to the middle layer giving rise to a vertical temperature gradient. The middle fluid in such cases acts as a heat sink. It has low temperature owing to no Joule heating and higher values of absolute velocity. However in figure 6b, the middle fluid acts as a heat source due to Joule heating and the end fluids act as a heat sink. Hence temperature of the middle fluid is higher than the end fluids. The temperature of the end fluids subsequently decreases to match the boundary condition at the walls.

S = 1 represents the case of external heat addition to the fluid layers from the walls. This gives rise to sharp temperature gradients in fluid 1 and fluid 3 in figure 6a. The temperature gradient is even higher in the middle fluid due to its low thermal conductivity. The temperature of the end fluids is higher than the middle fluid due to the effect of Joule heating as well. Very high values of Joule heating could have shifted the profile towards the case when S = 0. In figure 6b, the middle fluid is heated due to Joule heating; however it is not significant enough to raise its temperature over the end fluids which are being heated externally from the wall. Had the Joule heating been very significant, then we might have seen a temperature gradient reversal in the non-polar fluids.

(7a)

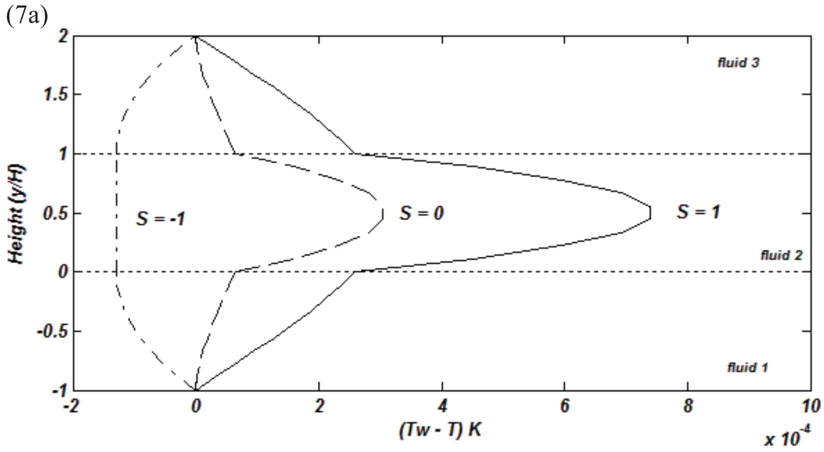


(7b)

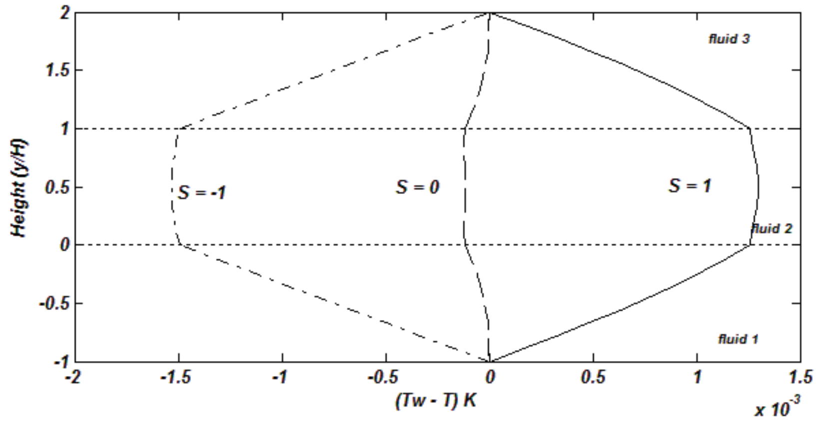


Figure 7: Plots for temperature profile with different values of S and P= - 0.05, (a) non polar fluid in the middle, k2/k1 = 0.1 (b) polar fluid in the middle, k1/k2 = 0.1

Figure 7 shows the results for P = -0.05. However, when we compare plots 7a and 7b, we observe lower values of absolute temperature difference between the wall and the fluid in the case where electroosmotic forces and that due to pressure gradient are opposing to each other (7a, P= -0.05). This can be explained by the energy conservation of the fluid control volume. Lower values of velocity have been observed in figure 4a for P= - 0.05. This implies a lower volume flow rate of the fluid. However, as the internal generations as well as the wall heat fluxes are same for figure 6a and 7a, the fluids get heated to a larger perceptible temperature in the latter case and hence have higher operating temperatures. This in turn reduces the temperature difference between the wall and the fluid. However, there is not much significant difference between figures 6b and 7b. The absolute velocity in figure 4b is much less than that in figure 4a. Hence P = 0.05 and P = - 0.05 does not create a significant change in velocity to cause any appreciable change in temperature. Higher negative values of P could have created an appreciable change in temperature.

### 3.4 Nusselt Numbers

Figures 8 and 11 represent the continuous variation of Nusselt number at the walls with the non-dimensional parameter P for various values of S. Nusselt numbers obtained at the two walls will be identical due to similar properties of the two end fluid layers. Hence, study of variation of Nusselt number at one wall will be sufficient. Lowest value of Nusselt number has been obtained for S = 0 in both figure 8a and 8b. This is because for S = 0, wall heat fluxes are effectively zero which gives a zero wall temperature gradient. As the bulk mean temperature difference is not zero, heat transfer coefficient almost equal to zero. This results in zero Nusselt number. In figure 8a, the value of Nusselt number that has been obtained for S = -1 is greater than that obtained for S = 1. This is because a greater difference between wall and bulk mean temperature is obtained for the latter case which implies a lower heat transfer coefficient for the same wall heat flux and Joule heating. The Nusselt number is almost constant throughout except near P = -0.063, there is a sudden fluctuation in Nusselt number both for S = 1 and S = -1. The sudden change in Nusselt number can be explained on the basis of figures 9 – 10.

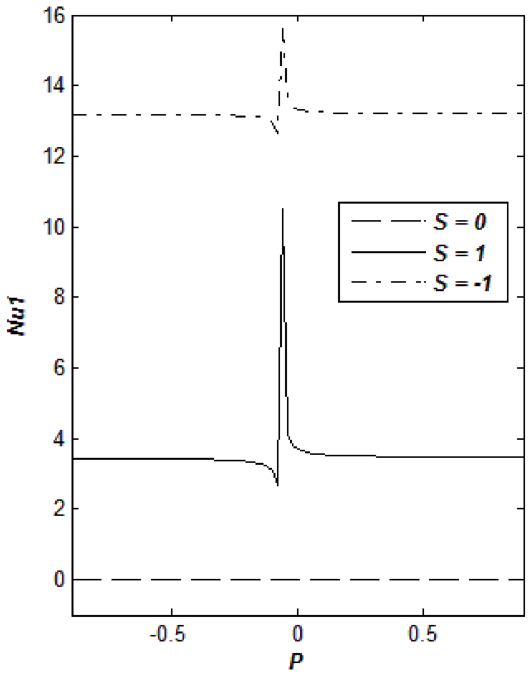


Figure 8: Variation of Nusselt number with P when non-polar fluid is in the middle

Figure 9 represents the variation of bulk mean temperature difference of the fluid with P for various value of S. It should be observed here that for P = 0, the temperature difference is equal to zero for all values of S. This is because at P = 0, both the electric field as well as the wall flux is zero. The general trend in figure 9a is due to the fact that as the value of P decreases, the velocity of the fluid decreases giving rise to increase in the fluid temperature. Again as P becomes more and more negative, there is flow reversal and velocity again increases in the reverse direction. Then the bulk temperature difference again begins to increase. However situation becomes critical when velocity of one or more fluid layer approaches zero as the pressure gradient and electric fields oppose each other. This point can therefore see sharp rise and fall of temperatures of one or more fluid layer thereby affecting the bulk mean temperature of the fluid. Temperature gradient remaining same, such strong fluctuation may manifest itself in the convective heat transfer coefficient and the resulting Nusselt number. Such a situation has occurred in 8. When resolution of the plot 9a was increased, a fluctuation in bulk mean temperature was observed (figure 9b) for S = 1. Similar phenomena can be observed for S = -1. In figure 10a, velocity plots have been provided near the region of fluctuation. As can be seen, near P = - 0.06, the velocity of the middle fluid layer becomes almost zero. Figure 10c which relates the discharge with P shows that the discharge reaches its minimum near this value of P. Figure 10b shows the temperature plots for S = 1. As can be seen, there has been a shift in temperature from negative to positive for S = 1 when heat is being added to the system. Initially for P = - 0.61, the fluid velocity of the middle layer nears zero giving rise to lower temperature difference between the wall and the fluid. As P increases more and more in the opposite direction, the flow is further decelerated which leads to further rise in temperature. At a point the temperature of the middle fluid becomes greater than the wall and it conducts heat to the end layers. However as these layers are themselves receiving heat from the wall, so there occurs a temperature inversion near the wall. Again, beyond a certain point the temperature becomes less than the wall. This occurs when the fluid gains velocity in the opposite direction.

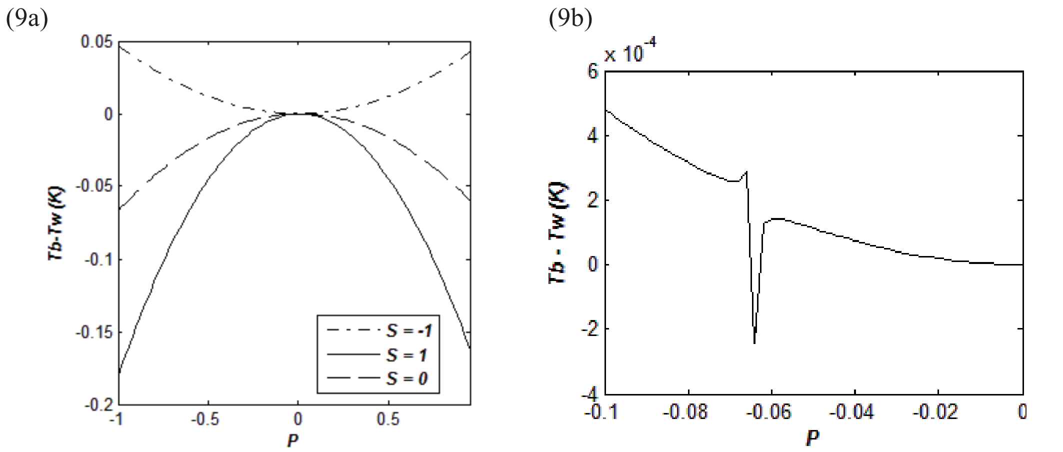


Figure 9: Variation of temperature difference with P (a) for different values of S (b) exploded view for S=1

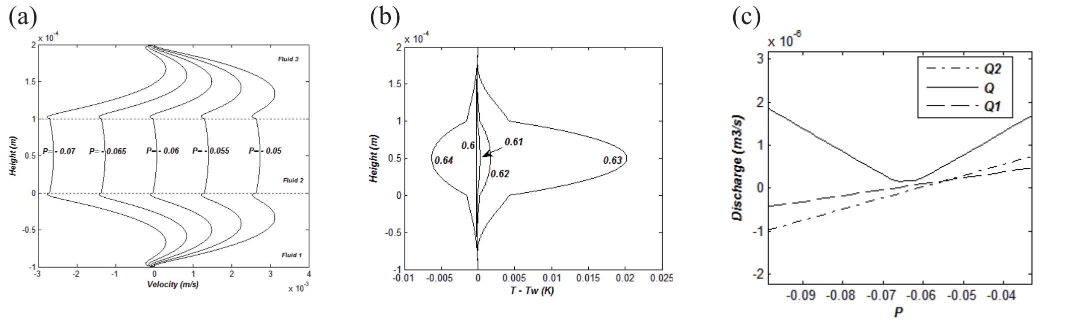


Figure 10: (a)Velocity profiles (b) Temperature profiles (c) Dischargefor S=1 and different values of P

A similar observation can be made with the reverse configuration. Here however, Nusselt number is higher for S = 1 than S = -1. This can be explained with the temperature profile of figure 6b and 7b. The bulk temperature difference is greater in case of S = -1 than in case of S = 1 giving rise to a low heat transfer coefficient and hence a low Nusselt number.

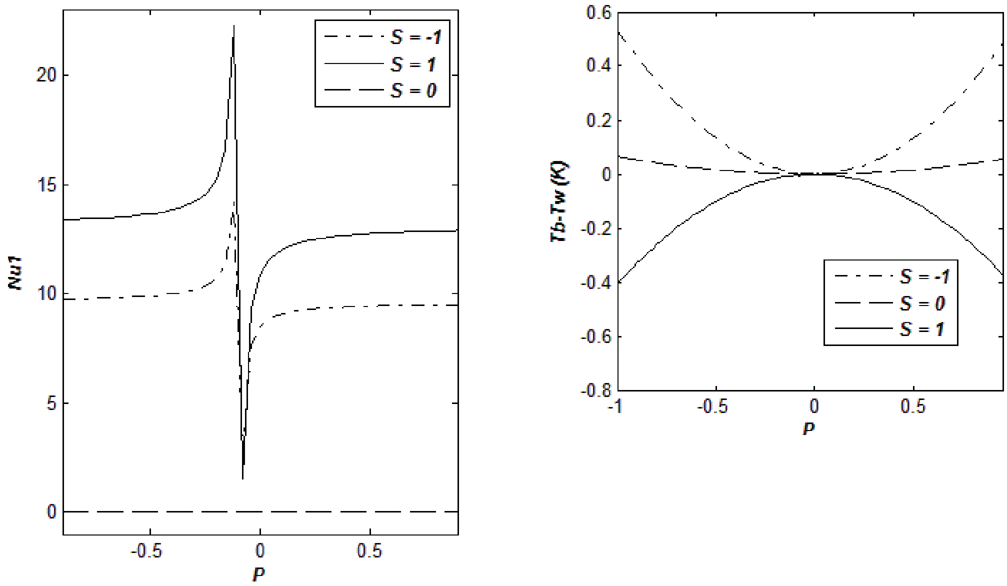


Fig.11 : Variation of Nusselt number and temperature difference with P

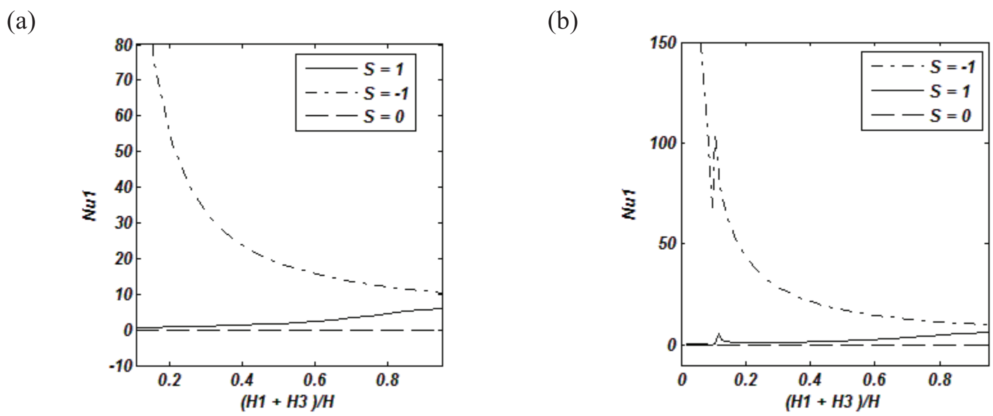


Figure 12: Variation of Nusselt number with relative height of fluid layers for (a) P = 0.5, (b) P = -0.5 with non-polar fluid in the middle

Figure 12a and 12b represent the variation of Nusselt number with variation in relative thickness of the conducting and non-conducting layer for P = + 0.5, - 0.5. The two conducting end fluid layers are of equal thickness. All other parameters have been kept constant. Nu = 0 has been obtained for S = 0 as wall heat fluxes are effectively zero. Also, the temperature plots show that lower wall temperature gradient is zero for S = 0. For S = 1, an increase in the Nusselt number has been observed with an increase in the conducting fluid layer thickness. The Nusselt number depends both on the variation of wall temperature gradients as well as the difference between the wall and bulk fluid temperatures. With increase in end fluid layers, the Joule heating also increases thereby increasing the bulk mean temperature of the fluid. Also, the wall temperature gradients decrease with an increase in the fluid layers. However, the decrease in wall temperature gradients occurs at a slower rate than that of the wall temperature difference. This results in an increase of heat transfer coefficient and the Nusselt number as well. For S = -1, the temperature of the fluid is greater than that of the wall. Due to Joule heating, this wall temperature difference increases with increase in conducting fluid layer thickness. However, the wall temperature gradient decreases with increase thickness of fluid layer resulting in the decrease of Nusselt number. It can be seen that there has also been a fluctuation in the Nusselt number when P = - 0.5. This is due to the fact that for a certain relative thickness of the fluid layers there has been a flow reversal which might have triggered sharp fluctuations in temperature and the resulting bulk mean temperature as well.

Figure 13 shows the variation of Nusselt number for polar fluid in the middle.

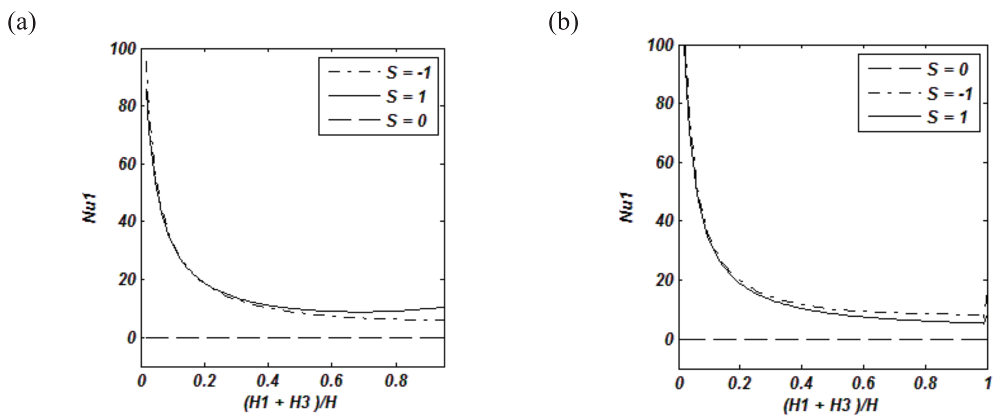


Figure 13: Variation of Nusselt number with relative height of fluid layers for (a) P = 0.5, (b) P = -0.5 with polar fluid in the middle

## 3. CONCLUSIONS

Combined pressure-driven and electroosmotic flow and heat transfer have been analyzed for fully developed flow in a microchannel with three immiscible fluids. Exact solutions have been obtained for velocity and temperature profiles and Nusselt number. The results are strongly affected by thickness of the fluid layers, applied forces and boundary conditions. These results are useful for control of flow and heat transfer of non-polar liquids in microchannels.

## NOMENCLATURE

| | |
|---|---|
| $C_p$ | Specific heat capacity |
| e | Electronic charge |
| E | External electric field |
| h | Heat transfer coefficient |
| H | Height of microchannel |
| k | Thermal conductivity |
| $k_b$ | Boltzmann constant |
| $n_\infty$ | Ionic number concentration in bulk fluid |
| Nu | Nuselt number |
| p | Pressure |
| q | Volume flow rate |
| q” | Heat flux per unit width |
| T | Absolute temperature |
| u | Flow velocity |
| z | Valence of ion |

$\alpha$ Thermal conductivity
$\phi$ Electric potential
$\kappa$ Debye-Huckel parameter
$\varepsilon$ Permittivity
$\zeta$ Zeta potential
$\mu$ Dynamic viscosity
$\rho$ Density
$\rho_e$ Electric charge density
$\sigma$ Electrical conductivity
$\theta$ Difference of fluid and wall temperature

## Subscripts

1 Lower fluid
2 Middle fluid
3 Upper fluid
w Wall
b Bulk mean
g Internal generation

## REFERENCES

[1] D. Burgreen, F.R. Nakache, Electrokinetic flow in ultrafine capillary slits, *J. Phys*. Chem. 68 (1964) 1084–1091.

[2] C.L. Rice, R. Whitehead, Electrokinetic flow in a narrow cylindrical capillary, *J. Phys*. Chem. 69 (1965) 4017–4024.

[3] S. Levine, J.R. Marriott, G. Neale, N. Epstein, Theory of electrokinetic flow in fine cylindrical capillaries at high zeta-potentials, *J. Colloid Interface Sci*. 52 (1975) 136–149.

[4] R.J. Yang, L.M. Fu, Y.C. Lin, Electroosmotic flow in microchannels, *J. Colloid Interface Sci*. 239 (2001) 98–105.

[5] R.J. Yang, L.M. Fu, C.C. Hwang, Electroosmotic entry flow in a microchannel, *J. Colloid Interface Sci*. 244 (2001) 173–179.

[6] L. Ren, D. Li, Electroosmotic flow in hetrogeneous microchannels, *J. Colloid Interface Sci*. 243 (2001) 255–261.

[7] N.A. Patankar, H.H. Hu, Numerical simulation of electroosmotic flow, *Anal*. Chem. 70 (1998) 1870–1881.

[8] P. Dutta, A. Beskok, T.C. Warburton, Electroosmotic flow control in complex microgeometries, *J. Microelectromech*. Systems 11 (2002) 36–44.

[9] C.Y. Yang, D. Li, J.H. Masliyah, Modeling forced liquid convection in rectangular microchannels with electrokinetic effects, *Int. J. Heat Mass Transfer* 41 (1998) 4229–4249.

[10] D. Maynes, B.W. Webb, Fully developed electro-osmotic heat transfer in microchannels, *Int. J. Heat Mass Transfer* 46 (2003) 1359–1369. 643

[11] D. Maynes, B.W. Webb, Fully developed thermal transport in combined pressure and electro-osmotically driven flow in microchannels, *J. Heat Transfer* 125 (2003) 889–895.

[12] D. Maynes, B.W. Webb, The effect of viscous dissipation in thermally fully developed electro-osmotic heat transfer in microchannels, *Int. J. Heat Mass Transfer* 47 (2004) 987–999.

[13] X.Y. Chen, K.C. Toh, C. Yang, J.C. Chai, Numerical computation of hydrodynamically and thermally developing liquid flow in microchannels with electrokinetic effects, *J. Heat Transfer* 126 (2004) 70–75. 652

[14] S. Chakraborty, Analytical solutions of Nusselt number for thermally fully developed flow in microtubes under a combined action of electroosmotic forces and imposed pressure gradients, *Int. J. Heat Mass Transfer* 49 (2006) 810–813.

[15] A.Q. Zade,M.T.Manzari, S.K. Hannani, An analytical solution for thermally fully developed combined pressure-electroosmotically driven flow in microchannels, *Int. J. Heat Mass Transfer* 50 (2007) 1087–1096.

[16] Z. Yang, X.F. Peng, B.X. Wang, Fully developed electroosmotically and hydrodynamically induced convection between two parallel plates, *Numer*. Heat Transfer Part – A 50 (2006) 905–926.

[17] A. Jain, M.K. Jensen, Analytical modeling of electrokinetic effects on flow and heat transfer in microchannels, *Int. J. Heat Mass Transfer* 50 (2007) 5161– 5167.

[18] A. Mukhopadhyay, S. Bannerjee, C. Gupta, Fully developed hydrodynamic and thermal transport in combined pressure and electrokinetically driven flow in a microchannel with asymmetric boundary conditions, *Int. J. Heat and Mass Transfer* 52 (2009) 2145-2154

[19] A. Brask, G. Goranovic, H. Bruus, Electroosmotic pumping of nonconducting liquids by viscous drag from a secondary conducting liquid, in: 2003 Nanotechnology Conference and Trade Show – Nanotech 2003, 2003, pp. 190–193.

[20] Y. Gao, T.N. Wong, C. Yang, K.T. Ooi, Two-fluid electroosmotic flow in microchannels, *J. Colloid Interface Sci*. 284 (2005) 306–314.

[21] Y. Gao, C. Wang, T.N. Wong, C. Yang, N.T. Nguyen, K.T. Ooi, Electro-osmotic control of the interface position of two-liquid flow through a microchannel, *J. Micromech*. Microeng. 17 (2007) 358–366.

[22] G.D. Ngoma, F. Erchiqui, Pressure gradient and electroosmotic effects on two immiscible fluids in a microchannel between two parallel plates, *J. Micromech*. Microeng. 16 (2006) 83–91.

[23] Y. Gao, T.N. Wong, J.C. Chai, C. Yang, K.T. Ooi, Numerical simulation of two-fluid electroosmotic flow in microchannels, *Int. J. Heat Mass Transfer* 48 (2005) 5103–5111.

[24] P.J. Stiles, D.F. Fletcher, Hydrodynamic control of the interface between two liquids flowing through a horizontal or vertical microchannel, Lab Chip 4 (2004) 121–124.

[25] S. Chakraborty, A. Garai, Micro-scale thermo-fluidic transport in two immiscible liquid layers subject to combined electroosmotic and pressure-driven transport, *Int. J. Heat Mass Transfer* 52 (2009) 2660-2666.

[26] L. Haiwang, T.N. Wong, N. Ngyuen, Time-dependent model of mixed electroosmotic/pressure-driven three immiscible fluids in a rectangular microchannel, *Int. J. Heat mass Transfer* 53 (2010) 772-785.